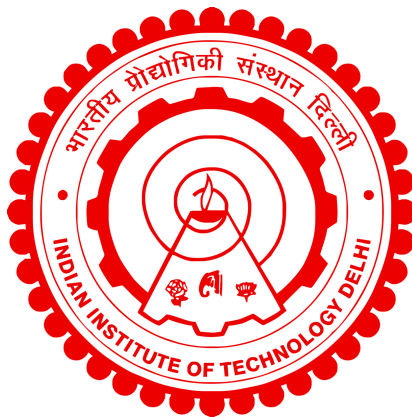


**FRACTURE MECHANICS OF BICRYSTAL
SILICON USING NEAR-TIP MECHANICS AT
THE ATOMISTIC SCALE**

SUNIL KUMAR DUTTA



**DEPARTMENT OF APPLIED MECHANICS
INDIAN INSTITUTE OF TECHNOLOGY DELHI**

JULY 2025

© Indian Institute of Technology Delhi (IITD), New Delhi, 2025

Fracture mechanics of bicrystal silicon using near-tip mechanics at the atomistic scale

by

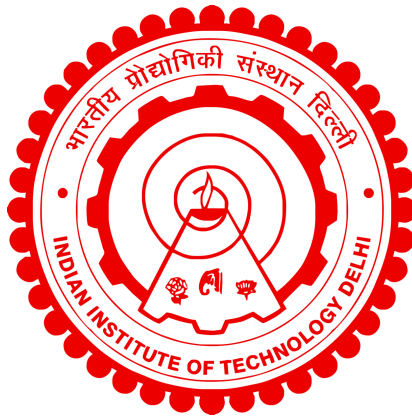
Sunil Kumar Dutta

Department of Applied Mechanics

Submitted

in partial fulfillment of the requirements of the degree of Doctor of Philosophy

to the



**INDIAN INSTITUTE OF TECHNOLOGY
DELHI**

JULY 2025

*Dedicated to my teachers who have enlightened and
motivated me*

Certificate

This is to certify that the thesis entitled “**Fracture mechanics of bicrystal silicon using near-tip mechanics at the atomistic scale**”, submitted by **Sunil Kumar Dutta (2019AMZ8723)** to the Indian Institute of Technology Delhi, for the award of the degree of **Doctor of Philosophy** in March, 2025, is a record of the original, bona fide research work carried out by him under our supervision and guidance. The thesis has reached the standards fulfilling the requirements of the regulations related to the award of the degree.

The results contained in this thesis have not been submitted in part or in full to any other University or Institute for the award of any degree or diploma to the best of our knowledge.

Prof. Gaurav Singh

Department of Applied Mechanics,
Indian Institute of Technology Delhi.

Acknowledgements

With profound humility, I offer my first and deepest gratitude to the Divine Providence, whose unseen hand has guided my steps and whose boundless grace has sustained me through every trial and triumph. In moments of uncertainty, He granted me strength; in moments of clarity, He bestowed wisdom. Without His blessings, this journey would have been but a distant dream.

I extend my heartfelt appreciation to my supervisor, Professor Gaurav Singh, whose support and guidance have been the cornerstone of this work. His mentorship has not only shaped this thesis but also refined my perspective as a scholar.

To my esteemed teachers and mentors, I am forever indebted. Your knowledge, encouragement, and dedication have been the guiding stars of my academic voyage.

To my family, whose unwavering love and sacrifices have been my greatest strength, I owe more than words can express. Your faith in me has been the foundation upon which this journey was built.

To my friends and colleagues, who have walked beside me, sharing both burdens and joys, your companionship has been a source of solace and inspiration.

Lastly, I acknowledge the silent yet powerful workings of time, perseverance, and providence itself, which have woven this endeavor into reality.

This thesis stands as a testament not merely to my efforts but to the support, wisdom, and kindness of all who have been part of this journey. To each of you, I offer my deepest and most sincere gratitude.

Abstract

Crack propagation and arrest are important phenomena in polycrystalline silicon. This phenomenon considerably affects the effectiveness of solar cells made up of polycrystalline silicon. To understand the crack propagation in polycrystalline silicon, it is essential to study the bicrystal first. Earlier, crack propagation has been studied in bicrystal materials primarily from the perspective of material behaviour. However, the mechanics part is largely missing. In the present work, crack propagation of bicrystal silicon during uniaxial tension has been studied at the atomistic scale. The silicon bicrystal was formed by joining two single crystals: crystal 1 and crystal 2 of different orientations. Various states like crack propagation initiation, propagation, arrest, re-initiation and crack/grain boundary (GB) interaction have been analysed using Stress Intensity Factor (SIF), calculated from the local crack tip virial stress field. Considering the effect of crack tip velocity, the dynamic SIFs at crack propagation state have been converted to the SIF of an equivalent static crack using the generalized expression for anisotropic material. It has been found that for the propagation state, crack propagation continues as long as the equivalent static SIF is greater than the critical SIF (CSIF). In crystal 1, crack propagation is along the low CSIF direction. Therefore, the crack did not change its path and propagated along a straight line. On the other hand, when the crack enters to crystal 2, it follows a zigzag path. Both of these observations have been justified in terms of near-tip calculated SIFs.

The mechanics of crack propagation initiation and crack/GB interaction does not remain same when the initial distance between crack tip and GB (DCG) is close to the GB ($DCG \leq 50 \text{ \AA}$). However, SIF cannot be calculated when crack tip is close to the GB ($DCG \leq 50 \text{ \AA}$). To overcome this limitation, ERR, evaluated using CTOD, has been used for all the analysis when crack tip is close to the GB. The CTOD determination is not an established method at atomistic scale. Hence, in the present work, ERR determined through CTOD will be verified for atomistic scale through atomistic and continuum scale J integral. J integral at atomistic scale is determined using volume integral method and verified by its path independence. It has been found that when the crack tip is close to GB ($DCG \leq 50 \text{ \AA}$), the crack propagation initiation occurs at lower ERR and remote strain. With the increase

in DCG, the crack propagation initiation happens at a higher ERR and strain. The effect of DCG becomes less relevant after a certain value, beyond which the crack propagation initiation resembles that of Single Crystal (SC). Further, the crack GB interaction and crack propagation in these bicrystals happened differently due to the different DCGs.

The difference in orientation of two crystal is called the tilt angle. With the variation of tilt angle, the crack propagation in crystal 2 also varies. When tilt angle is 1° , the crack propagation resembles to that of SC. With the increase of tilt angle to 20° the crack deflect into the crystal 2 and there is crack arrest at GB when tilt angle is 30° . Further increase of tilt angle till 45° shows gradual transition from crack deflection to zigzag crack propagation. When the tilt angle is again increased from 45° , crack deflection again started. The mechanics of crack/GB interaction is studied for all such case using near-tip SIF calculation and instantaneous crack tip velocity.

The results of bicrystal can be used to understand the mechanics of fracture in polycrystalline silicon. However, in this work, only phenomenological analysis has been done.

सारांश

पोलीक्रिस्टल सिलिकन में क्रैक का प्रसार और रोक महत्वपूर्ण घटनाएँ हैं। यह घटना पोलीक्रिस्टल सिलिकन से अब तक निर्मित सौर सेलों की प्रभावशीलता पर असर डालती है। पोलीक्रिस्टल सिलिकन में क्रैक प्रसार को समझने के लिए पहले बाईक्रिस्टल का अध्ययन करना आवश्यक है। अब तक बाईक्रिस्टल पदार्थों में क्रैक के प्रसार का अध्ययन मुख्यतः पदार्थ व्यवहार के दृष्टिकोण से किया गया है। परन्तु, यांत्रिकी संबंधी अध्ययन नहीं किया गया है। इस शोध में, एक दिशा के तनाव की स्थिति में बाईक्रिस्टल सिलिकॉन में क्रैक के प्रसार का परमाण्विक स्तर पर अध्ययन किया गया है। सिलिकन बाईक्रिस्टल के निर्माण हेतु दो भिन्न क्रिस्टल ओरिएंटेशन वाले सिंगल क्रिस्टल—क्रिस्टल १ एवं क्रिस्टल २—को आपस में संयोजित किया गया है। क्रैक प्रसार के प्रारंभ, प्रसार, रोक, पुनः प्रारंभ और क्रैक/ग्रेन बाउंड्री (GB) परस्पर-क्रिया जैसी विभिन्न अवस्थाओं का विश्लेषण स्ट्रेस इंटेन्सिटी फैक्टर (SIF) का उपयोग करके किया गया है, जो क्रैक टिप के करीब विरियल स्ट्रेस फील्ड के आधार पर मापा गया है। क्रैक टिप की गति को ध्यान में रखते हुए, क्रैक प्रसार की स्थिति पर प्राप्त डायनामिक SIF को समकक्ष स्टेटिक क्रैक के SIF में परिवर्तित किया गया है, जिसमें अनैसोट्रॉपिक पदार्थ के लिए सामान्यीकृत समीकरण का उपयोग किया गया है। यह पाया गया कि जब तक समकक्ष स्टेटिक SIF, क्रिटिकल SIF (CSIF) से अधिक होता है, क्रैक का प्रसार जारी रहता है। यह पाया गया है कि प्रसार अवस्था के लिए, क्रैक प्रसार तब तक जारी रहेगा जब तक समतुल्य स्टेटिक SIF CSIF से अधिक रहता है। क्रिस्टल १ में क्रैक प्रसार निम्न CSIF की दिशा में होता है। इसलिए, क्रैक ने अपना पथ नहीं बदला और सीधी रेखा के साथ प्रसारित होता गया। दूसरी ओर, जब क्रैक क्रिस्टल २ में प्रवेश करता है, तो वह जिग-जैग मार्ग का अनुसरण करती है। इन दोनों अवलोकनों की पुष्टि क्रैक टिप के करीब से प्राप्त SIF के आधार पर की गई है। जब क्रैक टिप और GB के बीच की प्रारंभिक दूरी (DCG) बहुत कम होती है ($DCG \leq 50 \text{ \AA}$), तब क्रैक प्रारंभ और क्रैक/GB परस्पर-क्रिया की यांत्रिकी समान नहीं रहती। इस स्थिति में SIF का माप संभव नहीं होता। इस बाधा को लांघने के लिए क्रैक टिप ओपनिंग डिस्प्लेसमेंट (CTOD) से प्राप्त एनर्जी रिलीज़ रेट (ERR) का उपयोग किया गया है। यद्यपि परमाण्विक स्तर पर CTOD के माध्यम से निर्धारित ERR पूर्णतः मान्य विधि नहीं है, इस लिए इस कार्य में प्राप्त मानों को परमाण्विक और कॉन्टिनोम स्तर पर आधारित J-इंटीग्रल के साथ जाँचा गया है। परमाण्विक स्तर पर J-इंटीग्रल वॉल्यूम इंटीग्रल विधि से निर्धारित किया गया है, और उसके पाथ इंडिपेंडेंस गुण को भी सत्यापित किया गया है। यह पाया गया है कि जब क्रैक टिप GB के बहुत पास होता है ($DCG \leq 50 \text{ \AA}$), तब क्रैक का प्रसार कम एनर्जी रिलीज़ रेट और कम स्ट्रेन पर आरंभ हो जाता है। जैसे-जैसे DCG बढ़ता है, क्रैक का प्रसार अधिक एनर्जी रिलीज़ रेट और स्ट्रेन पर आरंभ होता है। एक निश्चित दूरी के बाद, DCG का प्रभाव कम हो जाता है, और क्रैक का व्यवहार सिंगल क्रिस्टल जैसा हो जाता है। इसके अतिरिक्त, विभिन्न DCG मानों के कारण इन बाईक्रिस्टलों में क्रैक/GB की पारस्परिक-क्रिया तथा क्रैक का प्रसार अलग-अलग प्रकार से हुआ। दो क्रिस्टलों के ओरिएंटेशन में अंतर को झुकाव कोण कहा जाता है। झुकाव कोण के परिवर्तन के साथ, क्रिस्टल २ में क्रैक प्रसार भी परिवर्तित होता है। जब झुकाव कोण 90° होता है, तो क्रैक प्रसार सिंगल क्रिस्टल के समान ही होता है। झुकाव कोण के 20° तक बढ़ने पर क्रैक, क्रिस्टल २ में विक्षेपित हो जाता है और जब झुकाव कोण 30° होता है तो GB पर क्रैक रुक जाता है। जब झुकाव कोण 45° तक बढ़ता है, तब क्रैक का प्रसार विक्षेपण से जिग-जैग मार्ग की ओर धीरे-धीरे बदलता है। जब झुकाव कोण को 45° से ज़्यादा बढ़ाया

जाता है, तो क्रैक का विक्षेपण फिर से प्रारंभ हो जाता है। ऐसे सभी मामलों के लिए क्रैक/GB परस्पर-क्रिया की यांत्रिकी का अध्ययन टिप के करीब SIF माप और तात्कालिक क्रैक टिप वेग का उपयोग करके किया गया है। बाईक्रिस्टल के परिणामों का उपयोग पोलिक्रिस्टल सिलिकॉन में क्रैक-प्रसार की यांत्रिकी को समझने में किया जा सकता है। बहरहाल, इस शोध में केवल पोलिक्रिस्टल सिलिकॉन में क्रैक-प्रसार की घटनात्मक विश्लेषण को ही किया गया है।

Contents

Certificate	i
Acknowledgements	ii
Abstract	iii
Contents	vii
List of Figures	xi
List of Tables	xv
Abbreviations	xvii
Symbols	xix
1 Introduction	1
1.1 Problem statement	3
1.2 Literature review	4
1.2.1 An overview of macroscale mechanics	4
1.2.1.1 Virtual Crack Closure Technique	5
1.2.1.2 Cohesive Zone Modeling	6
1.2.1.3 eXtended Finite Element Method	7
1.2.2 An overview of microscale mechanics	9
1.2.3 An Overview of atomistic scale mechanics	10
1.2.4 Comparison of macroscale and atomistic scale simulations . .	12
1.2.5 Details of fracture mechanics using atomistic scale simulation	14
1.2.5.1 Fracture mechanics analysis in single crystal	15
1.2.5.2 Fracture mechanics analysis in bicrystal	17
1.2.5.3 Fracture mechanics analysis in polycrystal	18

Contents

1.2.6	Details to fracture parameters	18
1.2.6.1	Stress Intensity Factor	19
1.2.6.2	J integral	21
1.2.6.3	Crack Tip Opening Displacement	22
1.2.6.4	Energy Release Rate	23
1.3	Research gap	25
1.4	Objectives	28
1.5	Organization of Thesis	28
1.6	Summary	29
2	Methodology for atomistic simulation	31
2.1	MD simulation methodology	32
2.1.1	Inter-atomic potential	32
2.2	Validation of material properties	33
2.2.1	Single crystal silicon	33
2.2.2	Bicrystal copper	38
2.2.2.1	Validation of results for Cu bicrystal	44
2.3	Fracture properties at atomistic scale	47
2.3.1	Stress Intensity Factor	48
2.3.2	J integral	50
2.3.2.1	J integral in continuum domain	51
2.3.2.2	Limitation in the calculation of J integral at discrete domain	52
2.3.2.3	Formulation of J integral in discrete domain	53
2.3.2.4	Path independence of J integral at atomistic scale	55
2.3.3	Crack Tip Opening Displacement	56
2.3.3.1	Various approaches for CTOD evaluation	56
2.3.4	Energy Release Rate	58
2.3.4.1	Calculation of critical SIF and critical ERR from CTOD	59
2.4	Summary	60
3	Mechanics of Crack Propagation in Bicrystal Silicon	61
3.1	Simulation details	62
3.1.1	Methodology	62
3.1.2	Phases and states of the simulation	66
3.2	Physical, elastic and fracture properties of silicon	70
3.2.1	Physical properties	72
3.2.2	Elastic properties	72
3.2.3	Fracture properties	75
3.3	Determination of near-tip stress field	75
3.3.1	Validity of LEFM near crack tip	76

Contents

3.3.2	Details of FEM simulation	77
3.3.3	Analysis of near-tip stress field	79
3.3.3.1	For P1S1 state	79
3.3.3.2	For P1S6 state	79
3.3.3.3	For P1S2 state	80
3.4	Formulation for SIF calculation	81
3.4.1	SIF for moving crack	82
3.4.2	Determination of SIF along an arbitrary direction	87
3.4.3	Criteria for crack propagation	88
3.5	Results and analysis	88
3.5.1	Crack tip velocity	89
3.5.2	Phase 1: Crack propagation in crystal 1	92
3.5.3	Phase 2: Mechanics of crack/GB interaction	94
3.5.4	Phase 3: Crack propagation in crystal 2	96
3.5.4.1	Crack growth by void coalescence	98
3.5.4.2	Mechanics of zigzag path of crack propagation	99
3.6	Summary	101
4	Role of distance between crack tip and GB in the mechanics of crack/GB interaction	103
4.1	Simulation details	104
4.2	Determination of fracture properties of SC silicon	107
4.2.1	Limitation in SIF calculation	107
4.2.2	J integral and its path independence	109
4.2.2.1	Determination of J integral at continuum scale	113
4.2.2.2	Limitation of J integral calculation for bicrystal	113
4.2.3	Determination of ERR	114
4.3	Results & analysis	117
4.3.1	Mechanics of crack propagation initiation in bicrystal silicon for different DCG	117
4.3.2	Mechanics of crack/GB interaction in bicrystal silicon for different DCG	122
4.3.2.1	Crack/GB interaction in BC10	124
4.3.2.2	Crack/GB interaction in BC20	125
4.3.2.3	Crack/GB interaction in BC40	127
4.4	Summary	130
5	Effect of tilt angle in crack/GB interaction	131
5.1	Simulation details	132
5.2	Observation of results	133
5.3	Analysis of crack propagation and crack/GB interaction in bicrystals	136
5.3.1	SC silicon	136

Contents

5.3.2	BC01: tilt angle $\theta=01^\circ$	137
5.3.3	BC20: tilt angle $\theta=20^\circ$	141
5.3.4	BC25: tilt angle $\theta=25^\circ$	144
5.3.5	BC30: tilt angle $\theta=30^\circ$	146
5.3.6	BC45: tilt angle $\theta=45^\circ$	147
5.3.7	BC35, BC40 and BC60	147
5.3.8	Crack arrest and crack propagation from stress-strain plot . .	149
5.4	Summary	150
6	Conclusion	153
6.1	Fracture mechanics of polycrystal silicon	154
6.1.1	Generation of polycrystal structure	154
6.1.2	Phenomenological analysis of the simulation results	156
6.2	Conclusion	158
6.3	Future work	161
6.4	Summary	162
	Bibliography	163
	List of Publications	189
	Author Biodata	191

List of Figures

1.1	Schematic of crack closure model for 2D elements where a is the crack length, Δa is the increase of crack length and elements are represented by different boxes.	6
1.2	Schematic of lattice structure showing different planes in different colours are shown. The names of indicated planes are written below the lattice, which can also be verified from the mentioned co-ordinate system	16
1.3	Representation of CTOD (δ) at atomistic scale. The CTOD has been determined either by direct method or 90° blunt method and the circle represents the SSY zone ahead of the crack tip where $2r_y$ is the radius of the SSY zone. [1]	23
2.1	Flow chart for atomistic simulation showing important steps	35
2.2	OVITO image of simulation box for uniaxial test of SC silicon where the grey circles represent Si atoms. l , b and w are respectively length, breadth and width of the simulation box.	36
2.3	Schematic of lattice rotation. The lattice rotation is used to construct SC of different orientation.	40
2.4	Schematic of bicrystal copper where size of each SC is $144 \text{ \AA} \times 144 \text{ \AA} \times 144 \text{ \AA}$	41
2.5	OVITO image of bicrystal copper showing orientation of crystal 1, crystal 2 and GB	42
2.6	Variation of GB energy with GB width	45
2.7	The variation of overall stress σ_{22} with remote strain ϵ_{22}	46
2.8	Schematic of atoms and planes for the determination of SIF where the stress field along the crack i.e. along Layer 2 has been calculated by averaging stress of atoms in Layer 1 and Layer 3	49
2.9	Schematic of contour for calculating J integral. The J integral will be calculated using the area integral around annular area A whose inner radius and outer radius is respectively r_1 and r_2	52
2.10	OVITO image for the determination of CTOD using 90° blunt method of SC silicon at remote strain of 7.450%	57

List of Figures

2.11	Determination of CTOD using direct method for SC silicon at remote strain of 7.450%. Here, the dots represents atomic sites and CTOD is the distance between two straight lines at the crack tip.	58
3.1	a) Schematic of one lattice unit of silicon b) Schematic of edge cracked bicrystal structure subjected to uniaxial tensile test. L , b and w are respectively length, breadth and width of one SC. CS-1, CS-2 and CS-3 are respectively the orientation of crystal 1, crystal 2 and the bicrystal	64
3.2	2D view of silicon bicrystal in 1-2 plane, made using OVITO. Here, displacement boundary condition (Δ_b) is applied along the [010] direction	66
3.3	Variation of overall stress and remote strain of bicrystal silicon for different strain rates	67
3.4	Overall Stress-remote strain curve for bicrystal silicon for three different length ($2L$), i.e. $2L= 500 \text{ \AA}$, $2L= 1000 \text{ \AA}$, $2L=1500 \text{ \AA}$, for fixed height of $b=500 \text{ \AA}$	67
3.5	Important critical states of crack propagation in crystal 1 of bicrystal silicon a) initiation, b) propagation, c) arrest, d) re-initiation	69
3.6	Important states of crack propagation during the crack/GB interaction	70
3.7	Images show important states of crack propagation in crystal 2, where arrows represent the direction of crack propagation. Each state is identified from the simulation by the remote strain (ε_{22})	71
3.8	FE model image of bicrystal silicon showing initial crack, mesh, boundary condition and loading condition	78
3.9	Variation of normalized stress (σ_{22}/σ_0) with normalized distance from the crack tip ($r/2L$) in crystal 1 determined from MD and FEM, at a critical state just before propagation initiation (P1S1)	80
3.10	Variation of normalized stress (σ_{22}/σ_0) with normalized distance from crack tip ($r/2L$) from MD and FEM at the critical state just before re-initiation (P1S6)	81
3.11	Variation of normalized stress (σ_{22}/σ_0) with normalized distance from crack tip ($r/2L$) from MD and FEM at propagation P1S2	82
3.12	Co-ordinate system for stress transformation	87
3.13	Fitting of variation of crack tip extension with time (left) and plot of the variation of instantaneous crack tip velocity with time (right) from crack propagation initiation (P1S1) to arrest (P1S5) in crystal 1	90
3.14	Fitting of variation of crack tip extension with time (left) and plot of the variation of instantaneous crack tip velocity with time (right) from re-initiation (P1S6) to P2S9	90
3.15	Fitting of variation of crack tip extension with time (left) and plot of the variation of instantaneous crack tip velocity with time (right) for crack propagation in crystal 2	91

List of Figures

3.16	Fitting of variation of crack tip extension with time from P1S1 state in crystal 1 to crack propagation in crystal 2	91
3.17	Plot of the variation of instantaneous crack tip velocity with time from P1S1 state in crystal 1 to crack propagation in crystal 2	92
3.18	Schematic of zigzag crack path in crystal 2	97
4.1	Schematic of side edge cracked bicrystal structure where L_1 , L_2 and L_{12} are respectively the length of crystal 1, length of crystal 2 and the distance between the crack tip and GB. The initial crack length a_0 has been marked in dashed line and GB width Δ has been marked in grey band. The width and thickness of the structure are respectively b and w	105
4.2	Front view of bicrystal silicon taken from OVITO, where vertical column of black atoms in the middle represents the GB. Δ_b is the overall extension applied during the simulation. $2L$ ($= L_1 + L_2$) and b are respectively length and width of the simulation box	106
4.3	Atomic scale image of bicrystal showing crack tip close to the GB	108
4.4	Variation of atomistic J integral for SC silicon, determined from different volume integral, with $r_2 - r_1$, where $(r_2 - r_1)$ starts from 5 Å. Here, \bar{x}_5 , \bar{x}_{10} and \bar{x}_{15} are respectively mean of the data set along the solid-dashed line, solid line and dashed line and s_5 , s_{10} and s_{15} are respectively standard deviation of the data set along the solid-dashed line, solid line and dashed line	110
4.5	Variation of atomistic J integral for SC silicon, determined from different volume integral, with $r_2 - r_1$, where $(r_2 - r_1)$ starts from 10 Å. Here, \bar{x}_5 , \bar{x}_{10} and \bar{x}_{15} are respectively mean of the data set along the solid-dashed line, solid line and dashed line and s_5 , s_{10} and s_{15} are respectively standard deviation of the data set along the solid-dashed line, solid line and dashed line	111
4.6	Flow chart to show the validation process of ERR method using SC silicon	116
4.7	CTOD measurement for BC10 and BC20 bicrystals using 90° blunt method and direct method. Images on the left side are taken from OVITO and on right side are plotted using python.	118
4.8	CTOD measurement for BC40 and BC200 bicrystals using 90° blunt method and direct method. Images on the left side are taken from OVITO and on right side are plotted using python.	119
4.9	Variation of overall stress (σ_{22}) with remote strain (ε_{22}) for BC10, BC20, BC40 and BC200, showing crack propagation initiation point A,B,C and D, respectively	121
4.10	Images of different crack propagation states in BC10 near GB	123
4.11	Images of crack propagation in BC20	126
4.12	Images of crack propagation in BC40 near GB	128

List of Figures

5.1	Schematic of edge cracked bicrystal structure with θ as tilt angle . . .	133
5.2	Atomistic scale image of different bicrystals of varying tilt angle . . .	134
5.3	Crack propagation pattern for bicrystal with varying tilt angle. The tilt angle is shown in the top-right corner in angle mark	135
5.4	Fitting of variation of crack tip extension with time (left) and the variation of instantaneous crack tip velocity with time (right) for crack propagation in SC silicon	137
5.5	Fitting of variation of crack tip extension with time (left) and plot of the variation of instantaneous crack tip velocity with time (right) for crack propagation in BC01	138
5.6	Different states of crack propagation when crack propagating through the GB in BC01 where the crack tip is marked in red dot	139
5.7	Fitting of variation of crack tip extension with time (left) and plot of the variation of instantaneous crack tip velocity with time (right) for crack propagation in BC20	142
5.8	Different states of crack propagation when crack propagating through the GB in BC20	143
5.9	Fitting of variation of crack tip extension with time (left) and plot of the variation of instantaneous crack tip velocity with time (right) for crack propagation in BC25	144
5.10	Different states of crack propagation when crack propagating through the GB in BC25	145
5.11	Crack propagation path in BC35 and BC40	149
5.12	Variation of overall stress with remote strain for bicrystals with different tilt angle. The crowding of lines are shown sepaartely in rectangular box	150
6.1	Atomistic model of polycrystal silicon with 13 crystals where the side edge crack has length a_0 . Each grain boundary separating crystal i and j has been denoted as GB_{i-j}	155
6.2	Different states of crack propagation in polycrystal silicon	157

List of Tables

2.1	Comparison of the physical and mechanical properties of SC silicon using various interatomic potentials. The results determined in this study have been validated with the results from previous atomistic scale and experimental investigations.	38
2.2	Combined comparison of mechanical properties for Cu bicrystal . . .	45
3.1	Details of the observations made from the crack propagation in crystal 1. Each state is identified by remote strain (ε_{22}) and extension (Δ_b) . . .	68
3.2	Details of the observations made during crack/GB interaction. Each state is identified by remote strain (ε_{22}) and extension (Δ_b)	69
3.3	Details of the observations made from the crack propagation in crystal 2. Each state is identified by remote strain (ε_{22}) and extension (Δ_b) . . .	72
3.4	Material properties of SC silicon (orientation: [100][010][001]) for SW potential at 1 K temperature	74
3.5	Details of the calculations of CSIF with different number of atoms ahead of the crack tip ($K_{Ic}=1.013 \text{ MPa}\sqrt{\text{m}}$)	76
3.6	Static and dynamic SIF ahead of crack tip for different different states of crack propagation in crystal 1 along with other important parameters. K_{Ic} for crystal 1 along [100] direction is $1.013 \text{ MPa}\sqrt{\text{m}}$	93
3.7	Dynamic and equivalent static SIF ahead of crack tip for different states of crack propagation for crack GB interaction along with other important parameters	95
3.8	Static and dynamic SIF ahead of crack tip for different states of crack propagation for crystal 2 considering the effect of mixed mode fracture	97
4.1	Details of different bicrystal structure with varying distance between crack tip and GB (L_{12})	105
4.2	CTOD δ , J integral and ERR G for SC silicon at critical state just before crack propagation initiation	116
4.3	Percentage deviation of ERR (from CTOD) and atomistic J integral (J_{MD}) from continuum J integral (J_{FEM}) for SC silicon	116
4.4	Overall stress (σ_{22}), displacement (ΔL_y) and remote strain (ε_{22}) values at critical state just before crack propagation initiation and at crack/GB interaction for different bicrystal an SC silicon	120

List of Tables

4.5	CTOD δ , ERR G and J integral for different bicrystals and SC silicon at critical state just before crack propagation initiation	121
4.6	SIF for different states of crack propagation in silicon bicrystal BC10	125
4.7	SIF for different states of crack propagation in silicon bicrystal BC20	127
4.8	SIF for different states of crack propagation in silicon bicrystal BC40	128
5.1	Details of different bicrystal structure with varying tilt angle (θ)	132
5.2	Static and dynamic SIF ahead of crack tip for different states of crack propagation for BC01	140
5.3	Static and dynamic SIF ahead of crack tip for different states of crack propagation for BC20	142
5.4	Static and dynamic SIF ahead of crack tip for different states of crack propagation for BC25	146
6.1	Crystal orientation of polycrystal in Figure 6.1	156

Abbreviations

CS	C oordinate S ystem
CSIF	C ritical S tress I ntensity F actor
CZM	C ohesive Z one M odelling
CTOD	C rack T ip O pening D isplacement
DCG	D istance B etween C rack tip and G rain boundary
DSIF	D ynamic S tress I ntensity F actor
EPFM	E lasto P lastic F racture M echanics
ERR	E nergy R elease R ate
FE	F inite E lement
GB	G rain B oundary
LAMMPS	L arge-scale A tomic/ M olecular M assively P arallel S imulator
LEFM	L inear E lastic F racture M echanics
LSY	L arge S cale Y ielding
MD	M olecular D ynamics
OVITO	O pen V isualisation T ool
P1S1	P hase 1 S tate 1
SC	S ingle C ystal
SIF	S tress I ntensity F actor
SSY	S mall S cale Y eilding
SSIF	S tatic S tress I ntensity F actor
SW	S tillinger W eber
VCCT	V irtual C rack C losure T echnique
X-FEM	e Xtended F inite E lement M ethod

Symbols

σ_{av}	average crack tip stress
δ	CTOD
$\delta_{90^\circ\text{blunt}}$	CTOD by 90° blunt method
δ_{direct}	CTOD by direct method
G_δ	ERR for CTOD δ
σ_{22}	overall stress
σ_0	far field stress
ε_{22}	remote strain
K_I	Mode-I SIF
K_{II}	Mode-II SIF
K_{III}	Mode-III SIF
K_{Ic}	Critical SIF for Mode-I
K_{IIc}	Critical SIF for Mode-II
$K_I(t)$	Dynamic SIF for Mode-I
$K_{II}(t)$	Dynamic SIF for Mode-II
$K_I(0)$	Static SIF for Mode-I
$K_{II}(0)$	Static SIF for Mode-II
$V_2(p, q)$	pair potential
K_{eff}	effective SIF
$V_3(p, q, r)$	triplet potential
Δ	GB width
Δ_b	extension along the pulling direction
$2L$	length of simulation box
L_1	length of crystal 1
L_2	length of crystal 2
L_{12}	DCG

Symbols

b	width of simulation box
w	thickness of simulation box
v	instantaneous crack tip velocity
c_R	Rayleigh velocity
c_s	shear velocity
c_d	dilatation velocity
κ_1	universal stress function for Mode-I
κ_2	universal stress function for Mode-II
J_{MD}	J integral from MD
J_{FEM}	J integral from FEM
$G_{90^\circ\text{blunt}}$	ERR from 90°blunt method
G_{direct}	ERR from direct method
$G_{c/90^\circ\text{blunt}}$	critical ERR from 90°blunt method
$G_{c/\text{direct}}$	critical ERR from direct method
$G_{c/\text{discrete}}$	critical ERR from MD
$G_{c/\text{continuum}}$	critical ERR from FEM
G_c	critical ERR
$\delta_{90^\circ\text{blunt}}$	CTOD from 90°blunt method
δ_{direct}	CTOD from direct method
θ	tilt angle
GB_{1-2}	GB between crystal 1 and crystal 2